AAS 20-724

TRANSITIONS BETWEEN QUASI-PERIODIC ORBITS NEAR RESONANCES IN THE CIRCULAR RESTRICTED THREE-BODY PROBLEM

Stefano Bonasera*, Natasha Bosanac†

Natural transitions between near-resonant orbits occur throughout our solar system and are exploited during mission design. To study the vast solution space associated with these natural transitions, this paper focuses on constructing heteroclinic connections between families of quasi-periodic orbits near resonances in the Earth-Moon circular restricted three-body problem. The hyperbolic invariant manifolds associated with quasi-periodic orbits are examined using an alternative representation of a Poincaré map that is constructed using manifold learning, a technique used for dimension reduction, to simplify visualization and analysis. Initial guesses, identified from this map, are corrected and input to a continuation scheme to examine the existence of natural transfers with a similar geometry between various quasi-periodic orbits along each family. This approach and analysis is demonstrated for natural transitions from quasi-periodic orbits near the interior 3:2 resonance to quasi-periodic orbits near the exterior 1:2 resonance.

INTRODUCTION

Natural transitions between resonant and near-resonant orbits, existing in multi-body gravitational environments, are of much interest in astrodynamics and celestial mechanics. Recent missions such as the Interstellar Boundary Explorer (IBEX) and the Transiting Exoplanet Survey Satellite (TESS) missions leveraged orbits near the 3:1 and 2:1 resonances, respectively, in the Earth-Moon system.[1,2] In these scenarios, natural motion approaching or departing a specific resonance supplies low-cost transfers to new orbits for mission extensions or even an explanation for distinct changes in a natural trajectory during long-term analyses.[3] In the field of celestial mechanics, the natural transitions between resonances offer fundamental insights into the dynamical mechanisms governing small bodies throughout the solar system; examples include the transit of comet Oterma in the Sun-Jupiter system[4] and the "resonant sticking" of Kuiper Belt Objects (KBOs).[5]

Low-fidelity models, in combination with dynamical systems theory, provide an approximate, yet representative, framework to analyze the mechanisms governing resonance transitions in multi-body systems. For instance, the Circular Restricted Three-Body Problem (CR3BP) admits a variety of dynamical structures that are approximately retained in many higher-fidelity models of multi-body systems. In the CR3BP, heteroclinic connections between periodic or quasi-periodic orbits offer a rapid and informed approach to preliminary analysis of the fundamental mechanisms governing resonance transitions. The intersections between hyperbolic invariant manifolds from two different

*Ph.D. Student, Ann and H.J. Smead Aerospace Engineering Sciences, 3775 Discovery Dr., Boulder, CO, 80303, stefano.bonasera@colorado.edu.

†Assistant Professor, Ann and H.J. Smead Aerospace Engineering Sciences, 3775 Discovery Dr., Boulder, CO, 80303, natasha.bosanac@colorado.edu.

resonant or near-resonant orbits indicate the existence of heteroclinic connections. State-of-the-art approaches to rapidly identifying these intersections via dynamical systems techniques tend to leverage Poincaré maps to reduce the dimensionality of the problem. For instance, Koon et al. employ Poincaré maps to study the transit of comet Oterma in the Sun-Jupiter system via a comparison to the planar hyperbolic invariant manifolds of resonant orbits.[4] Later, Haapala and Howell extend this analysis by studying three-dimensional natural motion between these resonances.[6]

The set of bounded trajectories that exist near a resonance in the CR3BP includes both periodic and quasi-periodic orbits. Previous efforts in studying resonance transition tend to focus on trajectories connecting periodic motions obtained in approximate models, constraining the examined solution space. However, a recent approach presented by Olikara and Scheeres enables efficient numerical computation of quasi-periodic orbits.[7] This procedure also supports computation of the associated invariant hyperbolic manifolds, following a similar approach to that presented by Jorba.[8] With these tools, Olikara develops two techniques to calculate heteroclinic trajectories between two quasi-periodic orbits near libration points. In the first method, connections are constructed from a departing torus to an a posteriori defined arrival torus using arcs that remain bounded within a specified neighborhood of the secondary. In the second example, Olikara recovers a connection between two spatial quasi-periodic orbits via continuation from a heteroclinic connection between two nearby planar orbits.

To study the natural transitions between quasi-periodic orbits near resonances, this paper enhances traditional dynamical systems approaches to designing heteroclinic connections by employing data mining methods. A primary challenge in constructing spatial transfers in the CR3BP is that the resulting Poincaré maps are higher-dimensional; this task is even more challenging for the complex stable and unstable manifold structures associated with a torus. To effectively visualize the hyperbolic invariant manifold structures associated with quasi-periodic orbits via Poincaré mapping, a technique from Big Data is employed: manifold learning. Specifically, the higher-dimensional state information encoded in each map crossing is projected onto a lower-dimensional manifold that is calculated via the Uniform Manifold Approximation and Projection (UMAP) method. This unsupervised learning technique minimizes the topological distance between the high- and low-dimensional spaces.[9] Due to this theoretical foundation, UMAP has been used to study a wide variety of nonlinear systems, including visualizing complex proteins in single cell biology,[10] studying genetic structures in cohorts[11] and categorizing the origin of solar wind.[12]

This paper constructs natural transitions between quasi-periodic orbits near resonances in the CR3BP using dynamical systems theory and manifold learning. This approach is demonstrated through the design of natural transfers between spatial quasi-periodic orbits associated with the internal 3:2 and external 1:2 resonances in the Earth-Moon CR3BP. First, families of spatial quasi-periodic orbits near these two selected resonances are computed. Then, the hyperbolic invariant manifolds associated with two members of these quasi-periodic orbit families are calculated and reduced to a sequence of intersections with a surface of section. The resulting higher-dimensional crossings of the Poincaré map are projected onto a two-dimensional manifold that is calculated via UMAP. The crossings associated with the stable and unstable manifolds of the two quasi-periodic orbits are displayed using this alternative representation of a Poincaré map. Then, two crossings from each manifold structure, that are located nearby in the lower-dimensional space, are used to seed an initial guess for a heteroclinic connection. Since UMAP calculates a lower-dimensional embedding with a similar topological structure to the original higher-dimensional space, these two crossings are likely to be located nearby in the phase space; thus, this alternative representation

of a Poincaré map offers a useful starting point for identifying candidate arcs for constructing a heteroclinic connection. The discontinuous arcs are refined numerically to produce a continuous solution. Continuation is then used to compute a family of similar heteroclinic connections between other members of the same quasi-periodic orbit families. The resulting natural transfers supply preliminary insight into the existence and properties of natural transitions between quasi-periodic orbits near resonances in multi-body systems. Such insight is valuable for astrodynamicists to either leverage in low-cost transfer design in a multi-body system or to avoid distinct changes in the trajectory of a spacecraft over the lifetime of a mission. In celestial mechanics, such analysis also offers insight into the conditions that may lead to natural transits for comets and KBOs as well as an explanation of the associated dynamical mechanisms.

DYNAMICAL MODEL

This work leverages the CR3BP to model the motion of a point mass due to the gravitational influence of two primary bodies. In this model, two point mass primaries, P_1 and P_2, are assumed to move along circular orbits about their barycenter. The third body P_3, representing a spacecraft or a small body, is assumed to possess a negligible mass with respect to P_1 and P_2; P_3 is often referred to as test particle throughout this work.[13] Then, mass, length and time parameters are nondimensionalized. Following normalization, a mass parameter μ emerges to represent the ratio between the mass of the smallest primary and the total mass of the system; in the Earth-Moon system, $\mu \approx 0.01215$. In addition, a rotating orthogonal reference frame is defined by the right-handed unit-vector sequence $(\hat{\boldsymbol{x}}, \hat{\boldsymbol{y}}, \hat{\boldsymbol{z}})$. This frame rotates with the two primaries, enabling the construction of an autonomous set of equations of motion for the test particle. In this rotating frame, the $\hat{\boldsymbol{x}}$-axis is directed from P_1 to P_2, the $\hat{\boldsymbol{z}}$-axis is parallel to the orbital angular momentum of the system, while the $\hat{\boldsymbol{y}}$-axis completes the right-handed triad. The nondimensional state of the test particle is defined in the rotating frame and relative to the system barycenter as $\boldsymbol{x} = [x,\, y,\, z,\, \dot{x},\, \dot{y},\, \dot{z}]^T$. Then, the nondimensional equations of motion in the CR3BP for the test particle are written as

$$\ddot{x} - 2\dot{y} = U_x, \qquad \ddot{y} + 2\dot{x} = U_y \qquad \ddot{z} = U_z \tag{1}$$

where the pseudo-potential function is $U(\boldsymbol{x}) = (x^2 + y^2)/2 + (1-\mu)/r_1 + \mu/r_2$ and U_x, U_y and U_z denote the partial derivatives of U with respect to x, y and z, respectively. The distances of P_3 from the two primaries are $r_1 = \sqrt{(x+\mu)^2 + y^2 + z^2}$ and $r_2 = \sqrt{(x-1+\mu)^2 + y^2 + z^2}$. In this system, the Jacobi constant, an energy-like quantity, is defined as $JC(\boldsymbol{x}) = 2U(\boldsymbol{x}) - \dot{x}^2 - \dot{y}^2 - \dot{z}^2$.[13] At a fixed value of JC, a wide variety of fundamental solutions exist, including: five Lagrange points, labelled L_i for $i = [1, 5]$; periodic and quasi-periodic orbits; and chaos.

RESONANT ORBITS

The definition of a mean-motion orbital resonance is inherited from two-body dynamics, where two assumed massless test particles, B and C, are subject to the gravitational influence of a single point-mass central body, A. The test-particle B is in resonant motion with C when B completes exactly p orbits about A in the same time C revolves q times around A, with $p, q, \in \mathbb{N}^+$. The $p : q$ resonance is classified as interior when $p > q$ or exterior when $p < q$. When this definition is transitioned to the CR3BP, the body B is the test particle, body A is P_1 and C is P_2, e.g. the Earth and the Moon, respectively. However, body B possesses a non-negligible mass in the CR3BP, therefore the ratio between the periods of the test particle and P_2 in their motion around P_1 is only approximately equal to the $p : q$ ratio. In this paper, an initial guess for a planar $p : q$ resonant periodic orbit is

constructed using the two-body model. The obtained solution, which is not periodic in the CR3BP, is transformed into the barycentric rotating coordinate system. Differential corrections is then used to recover a periodic orbit in the CR3BP. Using this single periodic orbit, pseudo arc-length continuation is used to generate additional members of the same family of resonant orbits.[14–16]

The stability characteristics of a periodic orbit are used to gain insight into the nearby flow. A resonant orbit is uniquely defined by a state $\boldsymbol{x}(t) \in \mathbb{R}^6$ and orbital period T. Then, the State Transition Matrix (STM) $\Phi(t, t_0)$ supplies a linear mapping between a deviation from the initial state $\delta\boldsymbol{x}(t_0)$, to a deviation from a future state $\delta\boldsymbol{x}(t) = \Phi(t, t_0)\boldsymbol{x}(t_0)$. The monodromy matrix is defined as the STM evaluated over an orbital period, i.e., $[M] = \Phi(t_0+T, t_0)$. Spectral decomposition of the monodromy matrix produces six eigenvalues and associated eigenvectors.[17] Due to the symplectic nature of the underlying dynamical model, the monodromy matrix admits three pairs of reciprocal or complex conjugate eigenvalues. One trivial eigenvalue pair, associated with the periodicity of the orbit, always equals unity. For planar orbits, the remaining two pairs reflect the characteristics of nearby in-plane and out-of-plane motion: an eigenvalue with a magnitude larger than one is associated with the unstable mode; an eigenvalue with magnitude lower than one identifies the stable mode; and a complex conjugate pair of eigenvalues with unitary magnitude is associated with nearby oscillatory motion.[13]

Two fundamental motions emerge when a periodic orbit is perturbed along one of the nontrivial eigenvalues. When a single state along the orbit is perturbed along the locally stable (unstable) mode, the perturbed state $\boldsymbol{x}(t)$ produces a trajectory that naturally approaches the periodic orbit as $t \to +\infty$ ($t \to -\infty$). The collection of all the trajectories exhibiting this characteristic are labeled the stable (unstable) invariant manifold. Heteroclinic transfers exist when the stable and unstable invariant manifolds of two distinct periodic orbits intersect: these arcs naturally transfer the test particle between two periodic orbits in infinite time. When an oscillatory mode is excited, however, the perturbed state $\boldsymbol{x}(t)$ produces bounded oscillatory motion, i.e., a quasi-periodic orbit. The collection of every perturbed state presenting oscillatory motion comprises the central manifold.[18]

QUASI-PERIODIC ORBITS

A quasi-periodic orbit is a bounded trajectory that traces out the surface of an invariant torus; this paper focuses specifically on spatial tori governed by two fundamental frequencies. A state on the surface of a two-torus is described by two angular quantities $[\theta_1(t), \theta_2(t)]$, associated with the longitudinal and transverse directions, respectively. The associated fundamental frequencies, ω_1 and ω_2, of a bounded quasi-periodic orbit are incommensurate. This paper uses the approach presented by Olikara and Scheeres to compute quasi-periodic orbits in the CR3BP.[7,19] Olikara and Scheeres build their method upon previous studies from Jorba, Gómez and Mondelo by calculating the invariant curve associated with a torus via a stroboscobic mapping.[8,20] Then, an invariant curve $v(\cdot)$ represents an equilibrium solution of the mapping under the flow governed by Equation (1). After a stroboscopic mapping time $T = 2\pi/\omega_1$, a state $\boldsymbol{x}(\theta_1, \theta_2)$ that begins on the invariant curve undergoes a rotation on the curve by an angle $\rho = 2\pi\omega_2/\omega_1$. An invariance condition is then mathematically described as:

$$R_{-\rho} v\left(\boldsymbol{x}(\theta_1, \theta_2)\right) - \boldsymbol{x}(\theta_1, \theta_2) = \boldsymbol{0} \tag{2}$$

where $R_{-\rho}$ is a rotational operator. For computational efficiency, the invariant curve is approximated by a sequence of N points along the invariant curve, equally spaced in θ_2. These states are approximated via a truncated Fourier series. As a result, the operator $R_{-\rho}$ is transformed into a

combined sequence of matrices, $[R(-\rho)]$. By aggregating the points sampled along the invariant curve into a matrix as $[U] \in \mathbf{R}^{N\times 6}$, a numerical equivalent of the invariance condition becomes:

$$\boldsymbol{S} = \text{vec}([R(-\rho)]v\left([U](\theta_1,\theta_2)\right) - [U](\theta_1,\theta_2)) = \mathbf{0} \in \mathbf{R}^{6N} \tag{3}$$

where the condition is vectorized by the vec$(\cdot)$ operator. To compute an initial torus that lies close to a periodic orbit with oscillatory modes, a location $\boldsymbol{x}_0$ along the periodic orbit is defined, corresponding to a longitudinal angle $\theta_1 = 0$. The eigenvector $\boldsymbol{v}_C$, associated with the complex unitary eigenvalue λ_C of $[M]$, defines N points along an initial guess for an invariant curve as:

$$\boldsymbol{x}(\theta_1,\theta_{2,i}) = \boldsymbol{x}_0 + \epsilon(\text{Re}[\boldsymbol{v}_C]\cos\theta_{2,i} + \text{Im}[\boldsymbol{v}_C]\sin\theta_{2,i}) \tag{4}$$

where an odd number of equally spaced values of the transverse toroidal angle θ_2 are used and ϵ is a small scalar value. To construct the initial guess, the period of the underlying periodic orbit is used as an approximation for the stroboscopic mapping time T, while the rotational angle is approximated as $\rho = \text{Re}[-i\ln\lambda_C]$. The resulting initial guess, specified by the approximated states along the invariant curve $\boldsymbol{x}(\theta_1,\theta_{2,i})$, the stroboscopic time T and the rotational angle ρ, is corrected using the multiple-shooting formulation of the method presented by Olikara and Scheeres.[7] Q equally-spaced locations along θ_1 are identified to retrieve approximated invariant curves along the same torus, following Equation (4). Continuity at each mesh point and the invariance condition at the final node guide the torus correction process. Of course, as with many current numerical procedures for computing fundamental solutions, the tori that exist in the CR3BP are not exactly recovered due to the approximation introduced by the discrete Fourier transform, the small discontinuities between nodes, and the nonzero tolerance used to assess whether the constraint vector is satisfied. However, the resulting numerical solutions are expected to lie sufficiently close to the true solution. An additional constraint is incorporated to compute a one-parameter family of quasi-periodic orbits at a specified Jacobi constant. Then, pseudo-arclength continuation is employed to compute additional members of the quasi-periodic orbit family. In this paper, quasi-periodic orbit families are calculated using two formulations of a constraint on the energy level: 1) by constraining the exact Jacobi constant of each state on the invariant curve, to produce a result labeled a 'JC-family'; and 2) constraining only the average Jacobi constant of states along the invariant curve, producing members that are labeled a 'JC_A-family'. Each approach produces trajectories that could, potentially, be deemed members of the quasi-periodic orbit family at the specified energy level.

Once a quasi-periodic orbit has been computed, the linearized dynamical flow near a torus supplies useful information on the stability of the associated quasi-periodic orbit. Specifically, the stability of a torus is evaluated by inspecting the eigenstructure of the differential of the invariance condition, labeled $[DS]$. Following the work of Jorba, the eigenvalues of $[DS]$ correspond to concentric circles about the origin in the Gauss plane. Each of these circles is associated with a radius R in the complex plane. Analogous to the stability of periodic orbits, these radii exist in reciprocal pairs, and always includes the trivial radius $R = 1$. If non-unitary radii exist, the torus possesses stable and unstable modes. When the approximated invariant curve is perturbed along the locally stable (unstable) mode, the perturbed curve will naturally approach the torus for $t \to +\infty$ ($t \to -\infty$).[7] The collection of all the states naturally approaching (departing) the underlying torus in forward time is the stable (unstable) hyperbolic invariant manifold of the torus. This paper leverages the hyperbolic stable and unstable manifolds of different tori to compute natural transfers.

ENHANCING POINCARÉ MAP VISUALIZATION VIA DIMENSION REDUCTION

Poincaré Maps

In dynamical systems theory, Poincaré maps reduce the complexity of visualizing a large variety of trajectories by transforming a continuous solution into a sequence of discrete states. The first step in constructing a Poincaré map is defining a surface of section that is transverse to the flow of interest. There exist a variety of useful definitions of a surface of section to capture the flow in the CR3BP: events such as the minimum or maximum distance from a central body (i.e., apses); functions of state coordinates; and stroboscopic maps that capture the flow at specific constant times.[18] Once a surface of section has been defined, trajectories are propagated, either forward or backward in time, from a specified set of initial conditions. The intersections of these generated arcs with the surface of section are recorded and visualized in a lower-dimensional space via a Poincaré map. Selecting a surface of section is a key step in rapidly and thoroughly analyzing the underlying dynamics.[17] For instance, a well-constructed map may reveal the existence of patterns that correspond to specific types of fundamental motion, or the lack thereof.

Poincaré maps are a valuable technique for locating heteroclinic connections in the CR3BP, with an established record of success for planar periodic orbits. Following a similar methodology to Koon et al., consider two planar periodic orbits near the resonances of interest, as displayed in Figure 1(a). This figure displays periodic orbits in the interior 3:2 (magenta) and exterior 1:2 (blue) resonant orbit families in the Earth-Moon CR3BP at the same Jacobi constant of $JC = 2.73$. The Earth and Moon are indicated using gray circles, while the equilibrium points are indicated by red diamonds. These two periodic orbits each admit stable and unstable manifolds. To visualize these manifolds, a surface of section is defined as $y = 0$. Trajectories along the unstable manifold associated with the 3:2 resonant orbit and stable manifold associated with the 1:2 resonance are propagated, with up to 10 intersections in any direction with the surface of section recorded. Figure 1(b) displays these intersections of the unstable manifold of the 3:2 orbit (magenta) and the stable manifold for the 1:2 resonant orbit (blue) on a Poincaré map where each crossing is visualized in the $(x, \dot{x})$ plane. Each map crossing in this example is two-dimensional. Thus, each intersection between the curves formed out by the blue and magenta colored crossings indicates the existence of a heteroclinic connection that departs the 3:2 orbit and approaches the 1:2 resonant orbit. This heteroclinic connection is straightforwardly computed by locating two nearby crossings of the map – one from each hyperbolic invariant manifold – and correcting for continuity via multiple shooting.

When the trajectories of interest are spatial, the Poincaré map may appear as a dense set of higher-dimensional crossings that are challenging to analyze via a two- or three-dimensional projection. Gomez et al. study a four-dimensional Poincaré map by introducing two more constraints on the phase space variables at each crossings: the resulting bijective, two-dimensional visualization of the map is used to obtain transit trajectories with predefined behaviours.[21] Using a different approach, Haapala and Howell extend the planar investigation to analyse the path of temporally captured jovian comets in their spatial transit between distinct Sun-Jupiter resonances.[6] To aid visualization, they leverage glyph representations of multivariate data. Selecting nearby points on the map with similar glyphs, a discontinuous initial guess for a cometary transit is constructed and then corrected. In these examples, these approaches to Poincaré map visualization have led to new fundamental insights about dynamical mechanisms. In this paper, an alternative approach to visualization is presented to accommodate increasingly complex scenarios, while avoiding data obscuration, over-constraining the solution space and an increased workload for the human analyst. Specifically, manifold learning

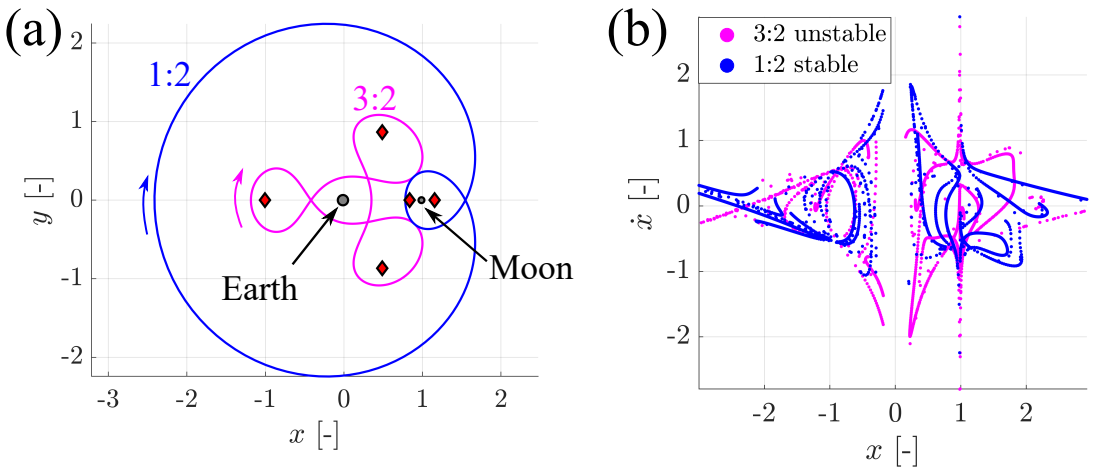

Figure 1. Examples of periodic orbits in the (a) 1:2 resonant family (blue) and 3:2 resonant family (magenta) in the Earth-Moon CR3BP at $JC = 2.73$ and (b) the intersections of the associated invariant manifolds with the $y = 0$ plane.

techniques are used to project higher-dimensional data associated with map crossings onto a lower-dimensional embedding. As a result, a human analyst may be able to rapidly and effectively analyze the solution space.

Manifold learning

Manifold learning techniques, such as the Uniform Manifold Approximation and Projection (UMAP), are a form of dimension reduction algorithms. Dimension reduction is founded in the premise that the descriptions used to form high-dimensional dataset contain redundant information and a key set of latent features exists.[9] UMAP, in particular, approaches this problem by constructing a low-dimensional representation of a nonlinear dataset to minimize the topological distance between the manifolds associated with the high- and low-dimensional descriptions. To implement this process, concepts from algebraic and fuzzy topology are leveraged. First, the algorithm assumes that the high-dimensional dataset is uniformly distributed on a local manifold; UMAP seeks to infer the Riemannian metric on the high-dimensional manifold that would result in such a distribution. Under the assumption of a locally connected manifold, UMAP leverages fuzzy simplicial sets to construct these local metrics and define a weighted graph that captures the fuzzy topological structure of the high-dimensional dataset. Then, the algorithm leverages optimization to identify a low-dimensional representation with a similar fuzzy topological structure to that of the high-dimensional dataset. UMAP initializes the lower-dimensional projection with spectral embedding techniques and then refines it by minimizing the cross entropy between the 1-simplicies of the high- and low-dimensional representations. This optimization step leverages stochastic gradient descent for computational efficiency. However, to support reproducibility of the results, the user can fix a random state for a minor increase in computational time. This algorithm is accessed in this work via the *umap-learn* library available in Python.

To apply UMAP to a particular dataset, several user-selected input parameters must be defined; the exact combination of selected parameters impacts the characteristics of the dataset projected onto the constructed lower-dimensional embedding. The three most significant input parameters include n_{neigh}, m_{dist} and n_{comp}: $n_{neigh} \in \mathbb{N}^+$ balances the local versus global structure in the dataset

with low values providing a final embedding favouring the local manifold structure; $m_{dist} \in [0, 1]$ balances the density level of the embeddings, ranging from low values and highly dense solutions to large values and sparse embeddings; and $n_{comp} \in \mathbb{N}^+$ defines the dimension of the lower-dimensional Euclidean representation. In this work, to aid the identification of regions where possible intersections between manifolds exist, large values of n_{neigh} and low values for m_{dist} are selected: this parameterization favors a compact visualization of the overall global structure, while also minimizing the effects of data obscuration. Moreover, the obtained datasets are projected into a two-dimensional Euclidean space to simplify visualization.

COMPUTING TRANSITIONS BETWEEN SPATIAL QUASI-PERIODIC ORBITS

This paper leverages data mining to construct natural transitions between quasi-periodic orbits near distinct resonances and at the same energy level. This methodology is comprised of two fundamental phases. The first phase focuses on constructing a discontinuous initial guess for a heteroclinic connection between two spatial quasi-periodic orbits. This phase begins by computing two families of quasi-periodic orbits near distinct resonances and at a constrained value of the Jacobi constant. The crossings of the hyperbolic manifolds associated with two selected members of these families with a common surface of section are used to generate a higher-dimensional Poincaré map. Then, UMAP is used to project the higher-dimensional crossings onto a low-dimensional representation. Using this alternative lower-dimensional representation of a Poincaré map, initial guesses for a heteroclinic connection are identified from nearby crossings of the two manifold structures. In the second phase, the initial guess is numerically corrected to produce one continuous natural transfer that connects two specific quasi-periodic orbits. This heteroclinic connection is then used in a continuation scheme to construct similar transfers between other members of each spatial quasi-periodic resonant orbit family.

Initial Guess Generation

Poincaré mapping and manifold learning are leveraged, in combination, to design an initial guess for a natural transition between spatial quasi-periodic orbits at the same energy level and near distinct resonances. The process used in this paper is summarized as follows:

1) *Compute each family of quasi-periodic orbits*: Two distinct planar resonant orbits at the same value of JC are selected. The orbits must admit both hyperbolic and center manifolds to ensure that a nearby family of quasi-periodic orbits exists and, through inheriting the stability of the periodic orbit, admit trajectories that naturally depart and approach the torus. The numerical approach presented by Olikara and Scheeres is used to calculate these two families of quasi-periodic orbits using each of the two formulations of the Jacobi constant constraint. This step produces two sets of families of quasi-periodic orbits near each resonance: a JC-family and a JC_A-family.

2) *Define the surface of section*: A surface is first defined to capture the flow associated with the hyperbolic invariant manifolds of the selected families of quasi-periodic orbits; in this work, a $y = 0$ plane is employed with no additional constraints on the sign of the velocity components at each crossing of the surface of section.

3) *Generate the Poincaré map*: One quasi-periodic orbit is selected from each family to possess a similar maximum out-of-plane component. The stable and unstable manifolds associated with each of the selected quasi-periodic orbits are generated using a small displacement

(equivalent to 50 km in the configuration space) along the stable and unstable eigenvectors, respectively. Then, up to 14 crossings with the surface of section are recorded. Since the hyperbolic invariant manifolds associated with these two quasi-periodic orbits tend to remain in the vicinity of the orbit for approximately 7 revolutions, only the 8th to 14th crossing of the manifolds with the surface of section are analyzed.

4) *Construct a lower-dimensional projection via UMAP*: The map crossings associated with the hyperbolic manifolds are used to form a six-dimensional dataset. UMAP is used to project the data onto a two-dimensional Euclidean space. The two input parameters used to govern UMAP are selected as $n_{neigh} = 200$ and $m_{dist} = 0.0$ to supply a compact representation that focuses on retaining the global structure of the Poincaré map crossings.

5) *Use the alternative representation of the Poincaré map to construct an initial guess*: An intersection between a stable and unstable manifold in the six-dimensional phase space indicates the existence of a heteroclinic connection. Recall that UMAP projects each intersection of these structures onto an lower-dimensional approximation of an underlying surface. Thus, two map crossings intersecting in the six-dimensional space may not exactly intersect in the lower-dimensional representation. However, since UMAP preserves the structure of the data, areas of the projected space where the hyperbolic manifolds have a low relative distances are investigated as candidate regions for locating heteroclinic connections. In these areas, two crossings (one from each of the stable and unstable manifolds) that lie nearby in the alternative representation are selected to construct an initial guess. These map crossings are propagated backward and forward in time to generate the associated unstable and stable manifold arcs, respectively. Then, five revolutions of the associated quasi-periodic orbits are concatenated to the beginning and end of the transfer to form a suitable initial guess.

This procedure for initial guess generation is demonstrated in this paper by constructing a transfer between spatial quasi-periodic orbits near the 3:2 and 1:2 resonances in the Earth-Moon CR3BP; thus, the transfer is constructed using the unstable manifold associated with a torus near the 3:2 resonance and the stable manifold associated with a torus near the 1:2 resonance.

Trajectory correction and continuation

The constructed initial guess is used to recover a family of continuous and natural transfers between spatial quasi-periodic orbits at the same energy level and near two distinct resonances. The corrections scheme is designed to: 1) ensure continuity between each hyperbolic invariant manifold arc; 2) ensure the transfer flows away from and into the selected tori; and 3) constrain the energy level. In this paper, a multiple shooting algorithm is formulated as an optimization problem that is implemented using Matlab's *fmincon* function. The objective function is designed to minimize the discontinuity between each torus and the transfer's initial and final states; along with equality constraints that enforce continuity and the energy level, solutions that minimize this objective below a specified threshold are deemed to sufficiently reflect a nearby heteroclinic connection. Of course, this procedure is conceptually equivalent to implementing a multiple shooting algorithm using only equality constraints. However, formulating this problem as an optimization problem is observed to exhibit less numerical sensitivity than a traditional Newton's method. Mitigation of the sensitivities observed in a traditional equality constraint formulation is an ongoing effort to be addressed in future work. Nevertheless, the presented approach supplies solutions that correspond to heteroclinic connections, within a numerical tolerance.

To define the optimization problem for implementing corrections, the free variable and constraint vectors are defined, along with the objective function. First, the initial guess is discretized into M nodes. To completely describe these nodes, the free variable vector is defined as

$$\boldsymbol{X} = [\boldsymbol{x}_1,\, \boldsymbol{x}_2,\, \ldots,\, \boldsymbol{x}_M,\, t_{1,2},\, t_{2,3},\, \ldots,\, t_{M-1,\,M}]^T \in \mathbb{R}^{7M-1} \tag{5}$$

with $\boldsymbol{x}_i$ for $i \in [1, M]$ representing the states at each node and $t_{j,\,j+1}$ denoting the propagation time from node j to node $j+1$. Each solution, described by this free variable vector, must satisfy continuity and energy constraints summarized by the constraint vector as:

$$\boldsymbol{F}(\boldsymbol{X}) = \left[JC(\boldsymbol{x}_1) - \bar{JC},\, \boldsymbol{x}_1(t_{1,2}) - \boldsymbol{x}_2,\, \boldsymbol{x}_2(t_{2,3}) - \boldsymbol{x}_3,\, \ldots,\, \boldsymbol{x}_{N-1}(t_{N-1,\,N}) - \boldsymbol{x}_M\right]^T \in \mathbb{R}^{6M+5} \tag{6}$$

where $\bar{JC}$ is the selected Jacobi constant. Then, the optimization problem is stated as:

$$\min_{\boldsymbol{X}} f(\boldsymbol{X}) \quad \text{s.t.} \quad \boldsymbol{F}(\boldsymbol{X}) = \boldsymbol{0} \tag{7}$$

for a scalar objective function $f(\boldsymbol{X})$. This objective function is designed to ensure minimization of the discontinuity between the terminal states along the transfer and the associated tori; conceptually, this corresponds to the requirement that the beginning of the transfer naturally flows away from the initial torus and the end of the transfer naturally flows into the final torus. Mathematically, this objective function is written as:

$$f(\boldsymbol{X}) = \|\boldsymbol{x}_1 - \boldsymbol{x}_{T1}\|^2 + \|\boldsymbol{x}_N - \boldsymbol{x}_{T2}\|^2 \tag{8}$$

where $\boldsymbol{x}_{T1}$ and $\boldsymbol{x}_{T2}$ represent the closest states along the associated torus to the initial and final states $\boldsymbol{x}_1$ and $\boldsymbol{x}_N$ along the transfer. Single shooting is leveraged to compute $\boldsymbol{x}_{T1}$ and $\boldsymbol{x}_{T2}$ at each iteration of the optimization scheme from the approximate invariant curves along the initial and final tori. For example, to evaluate the first term of the cost function, the closest invariant curve $[V](t_0)$ on the approximated departing torus to $\boldsymbol{x}_1$ at the beginning of the transfer is located. The single shooting algorithm is then used to obtain the closest point on the torus to $\boldsymbol{x}_1$, i.e. $\boldsymbol{x}_{T1}$. Specifically, the invariant curve $[V](t_0)$ is propagated for a time τ; the resulting approximated invariant curve at the end of this propagation, i.e. $[V](\tau + t_0)$, is rotated by an angle of α. Therefore, this single-shooting scheme uses a free variable vector $\boldsymbol{Y} = [\alpha,\, \tau] \in \mathbb{R}^2$. Then, the single shooting constrains the first state along this invariant curve to equal $\boldsymbol{x}_1$ via the constraint vector:

$$\boldsymbol{G}(\boldsymbol{Y}) = \boldsymbol{x}_1 - \text{vec}([R(\alpha)][V](\tau + t_0))|_1 = \boldsymbol{0} \tag{9}$$

The same procedure is repeated to evaluate the second term in the objective function using the arrival torus. This optimization problem is then solved using the MATLAB routine *fmincon*. While the JC-family is used to generate the heteroclinic transfer, only solutions that correspond to an objective below a value of 10^{-18} are considered to be sufficiently indicative of a heteroclinic connection: this threshold corresponds to an estimate of the position and velocity displacement from the departing and arrival torus of approximately 0.4 m and 10^{-3} mm/s. This is deemed reasonable given the impact of numerical errors in a relative long propagation in the CR3BP. When leveraging the JC_A-families to construct the heteroclinc connection, this threshold is raised to 10^{-12}, corresponding to an approximate displacement of 400 m and 1 mm/s. The increased threshold is due to the average Jacobi constant constraint in the generation process of the families and the fixed Jacobi constant throughout the transfer, as expressed in Equation (6). Of course, the original departing and arrival states that correspond to the stable and unstable manifold arcs may potentially

have a slightly different Jacobi constant; thus, an exact natural connection would be impossible to numerically generate.

Once the optimization strategy recovers a transfer between the two selected tori, a continuation scheme is used to generate similar transfers between other members of the two families of quasi-periodic orbits. This continuation approach follows a grid-like structure: initially, the departing torus is held fixed, while the arrival torus is gradually adjusted to step along the family. At each step of this continuation process, the transfer connecting one combination of tori is used to seed the initial guess for the next combination of tori. This process terminates when there are either no more members along the arrival torus family or a feasible transfer cannot be computed. Then, a similar procedure is repeated for each new departure torus. This procedure straightforwardly enables computation of a heteroclinic connection, with a similar geometry to the initial guess, between spatial quasi-periodic orbits along the two selected families. Note that this paper only seeks the existence of one transfer between each combination of quasi-periodic orbits and within the neighborhood of the initial guess. Similar solutions may also be generated by varying the departure and arrival locations along each torus. Such an analysis may also, potentially, expand the combinations of arrival and departure tori that admit a heteroclinic connection. Nevertheless, the implemented approach enables a preliminary analysis of the natural transitions between bounded motions near resonances. This complete procedure is demonstrated using spatial quasi-periodic orbits near the 3:2 and 1:2 resonances in the Earth-Moon CR3BP.

NATURAL TRANSITIONS BETWEEN TORI NEAR THE 1:2 AND 3:2 RESONANCES

In this section, natural transfers between two families of quasi-periodic orbits near resonances in the Earth-Moon CR3BP are constructed and analyzed. Specifically, the focus of this example is transfers from bounded motion near the 3:2 resonance to bounded motion near the 1:2 resonance. Following the technical approach outlined in the previous section, a point solution is constructed using Poincaré mapping and dimension reduction, in combination. This point solution is then used in a continuation scheme to recover similar transfers between other members of the quasi-periodic orbit families.

Recovering a Point Solution

Families of quasi-periodic orbits near each of the 3:2 and 1:2 resonances are generated in the Earth-Moon CR3BP. First, the planar resonant orbits depicted in Figure 1(a) are employed to compute the family of associated quasi-periodic orbits. These planar 3:2 and 1:2 resonant orbits exist at a Jacobi constant of $JC = 2.73$ with a period of ≈ 55.92 days and ≈ 50.54 days, respectively; at this energy level, periodic orbits in both families admit planar stable and unstable manifolds and a spatial center manifold. Families of quasi-periodic orbits are then generated at this same Jacobi constant. To construct an initial guess for torus computation, a perturbation of $\epsilon = 5 \times 10^{-5}$ in Equation (4) is used to step along the eigenvector associated with the oscillatory mode. Then, each torus is computed using $N = 25$ states along the invariant curve and $Q = 3$ patch points along the orbit. Using the torus computation method presented by Olikara and Scheeres, two sets of quasi-periodic orbits are constructed for each resonance: one corresponding to a JC-family and another corresponding to a JC_A-family. To compare the geometrical differences, 20 members per family are generated and represented using a color scheme that is consistent with Figure 1(b). Figure 2(a) displays one of the first members of the 1:2 family at the top; below this torus, the last members of the JC- and JC_A-families are plotted. While the initial members of the JC-family are geo-

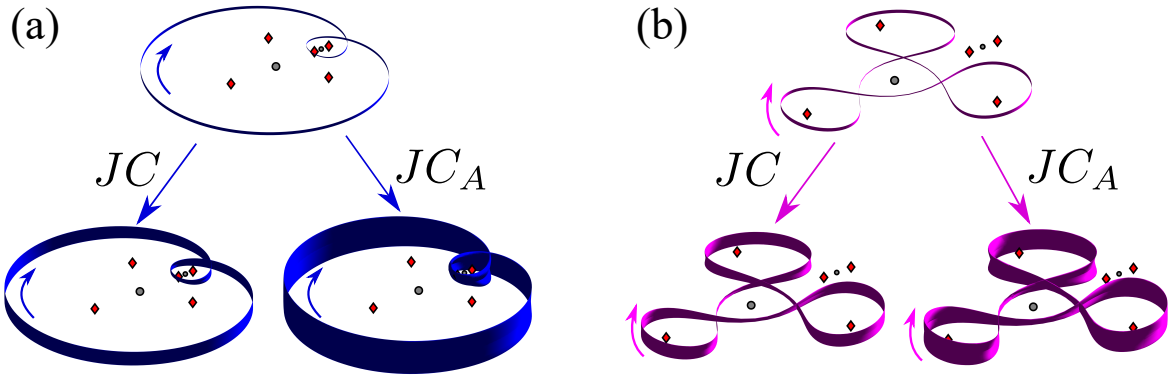

Figure 2. Example tori along the JC- and JC_A-families in the Earth-Moon CR3BP at $JC = 2.73$ for (a) 1:2 family of quasi-resonant orbits (blue) and (b) 3:2 family of quasi-resonant orbits (magenta).

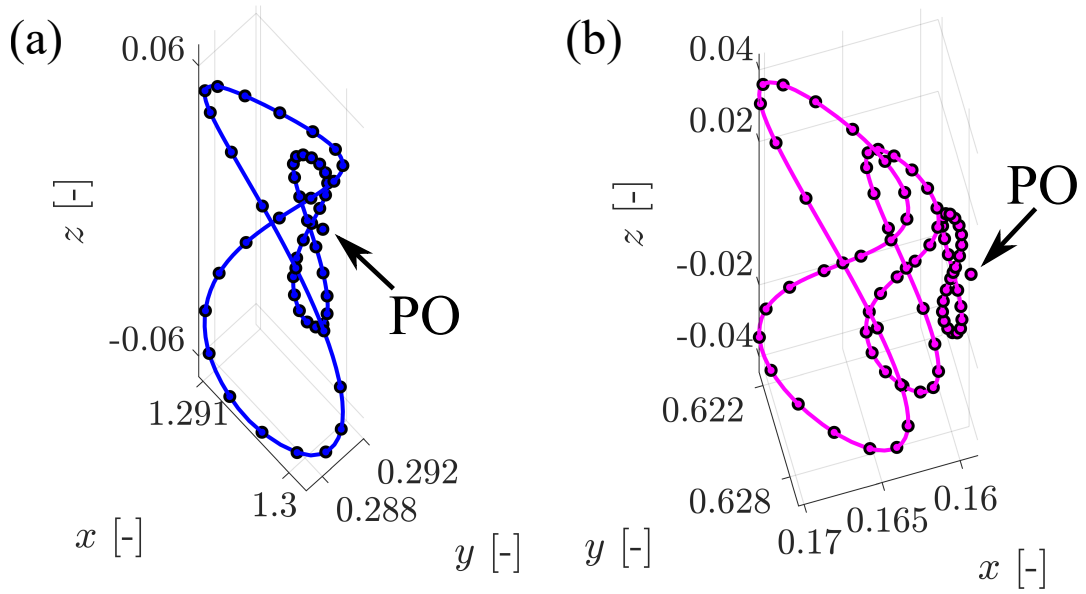

Figure 3. Sample invariant curves projected onto the configuration space for selected tori in the Earth-Moon CR3BP at $JC = 2.73$ for the (a) 1:2 (b) and 3:2 JC-families.

metrically equivalent to the associated JC_A members, the difference becomes evident at the family extrema: the last computed member of the JC_A-family, for the specific discretization used, extends twice as far out of the plane of the primaries as the last member of the JC-family. Similarly, Figure 2(b) displays similar information for the 3:2 resonant quasi-periodic orbit family. Each figure indicates the Earth and the Moon as gray circles, together with the Earth-Moon Lagrange points as red diamonds. Then, Figure 3(a) displays sample invariant curves associated with a few members of the 1:2 JC-family of quasi-periodic orbits: the figure reports as blue markers the states used to approximate the invariant curves, as well as the fixed point associated with the nearby periodic solution. Figure 3(b) supplies similar information for the 3:2 quasi-periodic orbit family.

A point solution for a natural transfer is constructed using the unstable manifold of a quasi-periodic orbit near the 3:2 resonance and the stable manifold associated with a torus near the 1:2

resonance. Specifically, this transfer is constructed between the last members of the JC-family, displayed in Figure 2(a-b). The unstable manifold of the quasi-periodic orbit near the 3:2 resonance and the stable manifold of the quasi-periodic orbit near the 1:2 resonance are generated using invariant curves at 101 values of θ_1, i.e., in the longitudinal direction along the quasi-periodic orbit. The manifolds associated with each torus are calculated using an initial displacement of 50 km along the associated unstable/stable eigenvectors of the $[DS]$ matrix used during torus construction. These manifolds are propagated for up to 14 returns to the $y = 0$ surface of section, in any direction; recall that the first 7 map crossings for each trajectory are excluded from this analysis as they tend to remain close to the quasi-periodic orbit. These selected intersections of the manifolds with the surface of section produce a total of 40,239 and 38,934 crossings for the 3:2 and the 1:2 resonances, respectively. Figure 4(a) displays the intersections of the generated subset of the invariant manifolds with the $y = 0$ surface of section via a projection onto the $[x, \dot{x}]$ plane. In this projection, the manifolds associated with the quasi-periodic orbits resemble the crossings of the stable and unstable manifolds associated with the planar periodic orbits in Figure 1(a). However, the increased complexity of these four-dimensional map crossings becomes apparent in a three-dimensional projection on the $[x, \dot{x}, z]$ space, as depicted in Figure 4(b); the manifolds possess a significant out-of-plane component. Both the two-dimensional and three-dimensional representations do not completely represent the higher-dimensional intersections of the invariant manifolds with the surface of section. Thus, two map crossings that are located nearby in either of these two- or three-dimensional projection may not be close in the full six-dimensional phase space. Including a fourth dimension or introducing further constraints in the problem could mitigate this problem. However, including a fourth dimension would further complicate the visualization and analysis of the Poincaré map, while the design space would significantly shrink with additional constraints.

UMAP is employed to reduce the complexity of visualizing a large set of four-dimensional data via a projection onto a two-dimensional Euclidean space. The map crossings associated with both the stable and unstable manifolds are combined to form the complete dataset that is input to UMAP. The input parameters for UMAP are selected as $n_{neigh} = 200$ and $m_{dist} = 0.0$; using these values, UMAP produces a projection onto a two-dimensional space as displayed in Figure 5. The projection

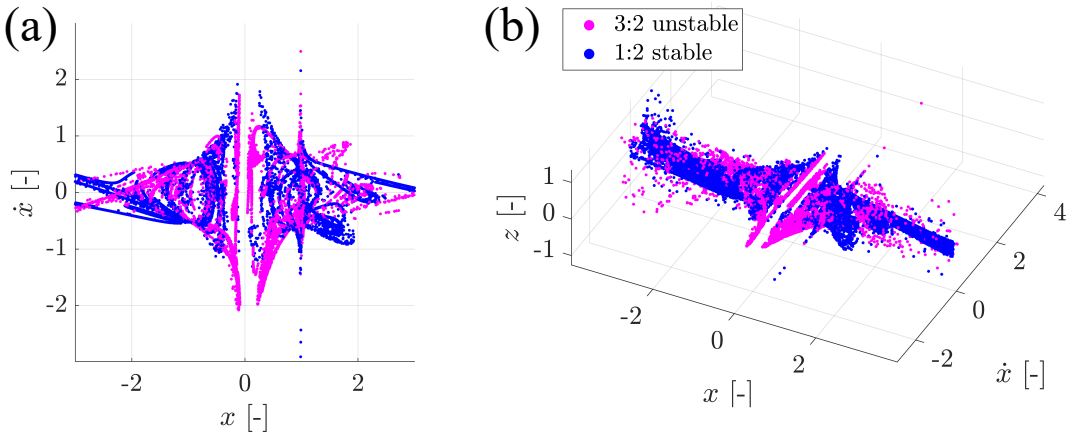

Figure 4. Poincaré map of the hyperbolic invariant manifolds associated with the intersections of the selected tori with the $y = 0$ plane in the 1:2 (blue) and 3:2 (magenta) quasi-periodic orbit family at $JC = 2.73$: (a) projection onto the $(x, \dot{x})$ plane and (b) projection onto the $(x, \dot{x}, z)$ space.

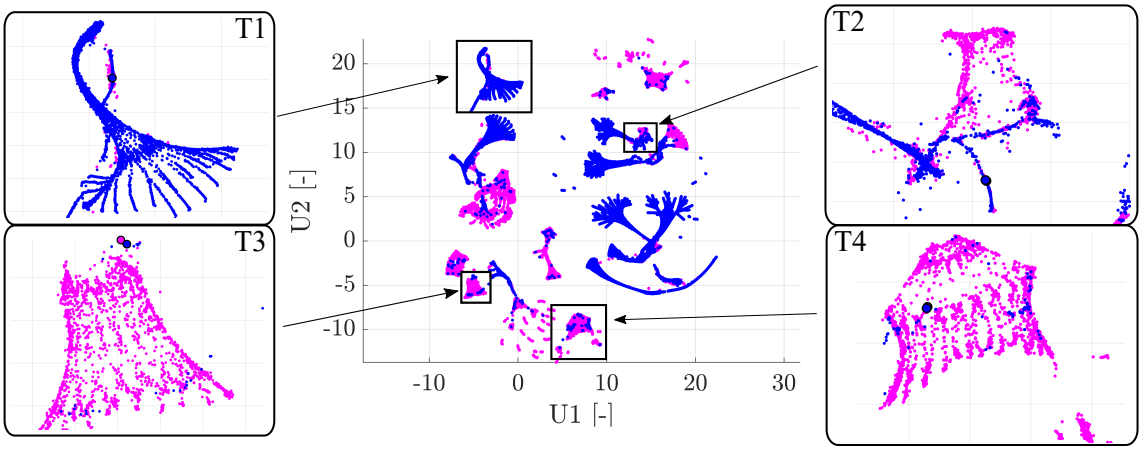

Figure 5. Center: projection of the invariant manifold dataset in Figure 4 onto the two-dimensional Euclidean space calculated by UMAP. Boundaries: zoomed-in perspectives of four regions of intersections between the stable and unstable manifolds of each quasi-periodic orbit.

of the entire dataset is depicted in the center of this figure; the blue markers indicate map crossings of the stable manifold associated with the quasi-periodic orbit near the 1:2 resonance, while the magenta markers correspond to the unstable manifold associated with the quasi-periodic orbit near the 3:2 resonance. The two axes, labeled $U1$ and $U2$, correspond to two variables that define the two-dimensional space calculated by UMAP to produce a similar fuzzy topological structure to that of the higher-dimensional data. Recall that, in this computational procedure, the projection calculated by UMAP preserves the structure of the data, but not the density. As a result, two map crossings that are close in the full phase space are expected to be located nearby in the two-dimensional projection. Analysis of this projection at the center of Figure 5 reveals that there are multiple regions of both blue and magenta points where the stable and unstable manifolds may potentially cross the $y = 0$ surface of section with similar state vectors. It is these regions that are used to straightforwardly identify suitable map crossings to generate an initial guess for a nearby continuous transfer between the two quasi-periodic orbits. Four interesting regions appear in the zoomed-in plots at the boundaries of Figure 5 and are used to generate four distinct transfers. Additional regions of overlapping magenta and blue point clouds that appear in the center of Figure 5 are identified and may enable the construction of natural transfers of alternative geometries.

Each of the four regions of overlapping map crossings on the two-dimensional projection calculated by UMAP is used to generate point solutions for a natural transition between quasi-periodic orbits associated with the 3:2 and 1:2 resonances in the Earth-Moon CR3BP. Within each of the zoomed-in regions displayed at the boundaries of Figure 5, map crossings that exist nearby on the projected space are selected from each of the unstable manifold associated with the quasi-periodic orbit near the 3:2 resonance and the stable manifold associated with the quasi-periodic orbit near the 1:2 resonance. As described in the previous section, each pair of map crossings is propagated towards the generating quasi-periodic orbit. Five revolutions around the quasi-periodic orbits are appended to the beginning and end of the transfer to generate a discontinuous initial guess. The numerical corrections procedure described earlier is implemented to recover a nearby natural transfer, as displayed in Figure 6. In this figure, each transfer is labeled to correspond to the associated zoomed-in view in Figure 5, marked by the identifier T1 to T4. Each of the depicted transfer is cal-

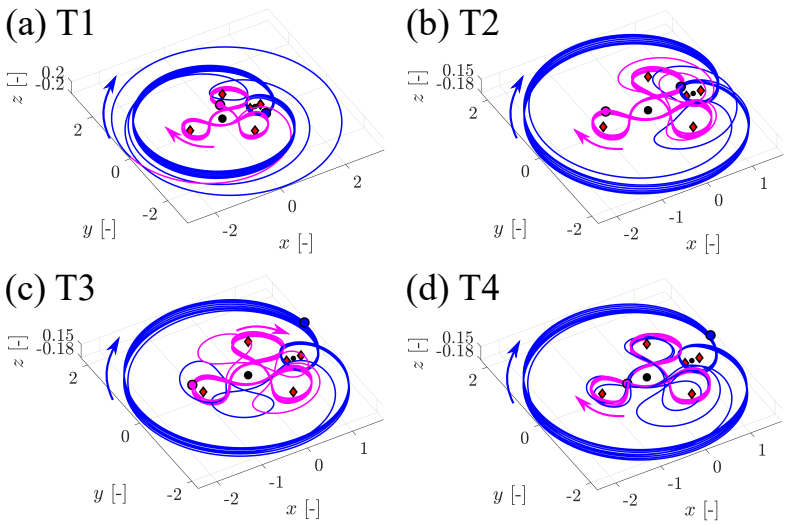

Figure 6. Selected natural transfers between quasi-periodic orbits in the 1:2 and 3:2 resonant orbit families. The transfers are labeled by the region in Figure 6 used to identify suitable map crossings.

culated with a value of the objective function, used to assess whether the trajectory has flowed into or away from the quasi-periodic orbits, equal to $f(\boldsymbol{X}) \approx 10^{-18}$, and satisfying the dynamics and adjunct constraints with $\|\boldsymbol{F}(\boldsymbol{X})\| \approx 10^{-13}$ in a computational time of approximately 15 seconds per trajectory. Furthermore, each transfer lies close to the initial guess. The selected transfers each begin at the magenta circle marker on the quasi-periodic orbit associated with the 3:2 resonance and terminate at the blue circle marker on the quasi-periodic orbit associated with the 1:2 resonance. Each trajectory is colored in magenta for the portion of the transfer corresponding to the first quasi-periodic orbit and the unstable manifold arc; the rest of each trajectory is colored in blue. These point solutions for natural transitions between the two selected quasi-periodic orbits each exhibit a slightly different geometry due to the specific manifold arcs used to construct the initial guess. The intersections of these trajectories with the surface of section at $y = 0$ are displayed in the traditional Poincaré map representation in Figure 7. The general set of intersections of the 3:2 unstable manifold (magenta) and the 1:2 stable manifold (blue) in Figure 4 are displayed as transparent, while the intersections of the T1 to T4 transfers appear in gray. This figures supplies further verification that constructed transfers lie near the intersections of the two manifolds on the surface of section in the traditional representation of a Poincaré map.

Family continuation

Continuation is used to generate similar natural transfers across multiple quasi-periodic orbits within each of the JC-families at $JC = 2.73$ near the 3:2 and 1:2 resonances. To demonstrate this approach, consider the natural transfer T1 in Figure 6(a). Continuation is applied to compute transfers with a similar geometry between unique combinations of quasi-periodic orbits; note, continuation is not used to find similar transfers connecting the tori at various longitudinal and transverse angles. Following application of this continuation procedure, Figure 8 presents a summary of the computed natural transfers for this particular transfer geometry from quasi-periodic orbits near the 3:2 resonance to quasi-periodic orbits near the 1:2 resonance. In the top-right plot of this figure, the horizontal and vertical axes depict the maximum out-of-plane component of the position vector at

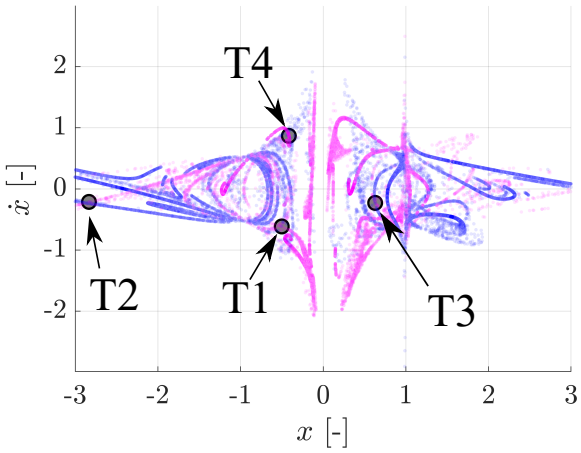

Figure 7. Crossings of the transfers (gray) in Figure 6 overlaid on the Poincaré map of the hyperbolic invariant manifolds from the selected quasi-periodic orbits in the 1:2 (blue) and 3:2 (magenta) resonant orbit families at $JC = 2.73$, using a surface of section at $y = 0$.

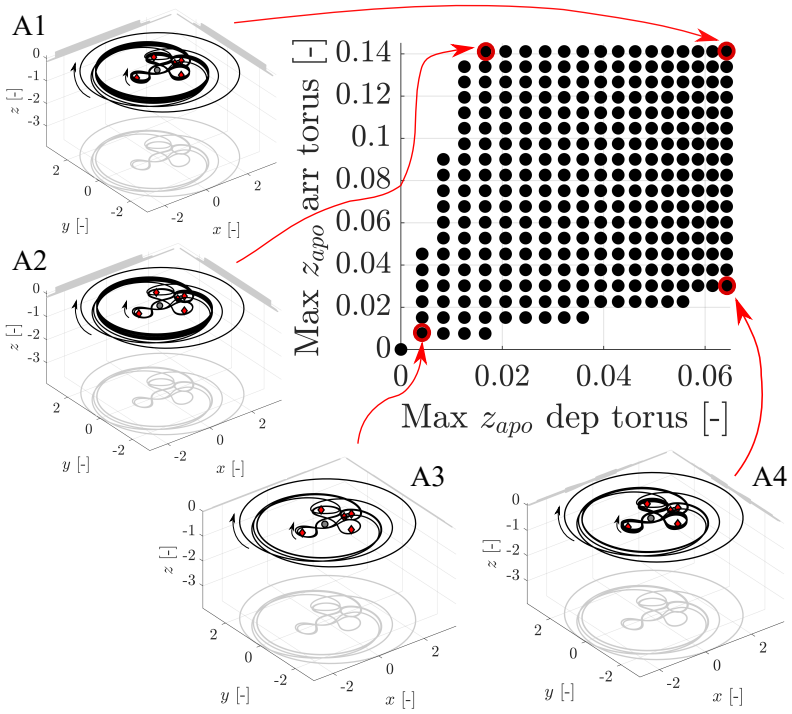

Figure 8. Summary of the T1 natural transfers continued from Figure 6(a). Each black marker indicates a transfer from a departing 3:2 quasi-periodic orbit and an arrival 1:2 quasi-periodic orbit in the JC-families, each identified by the maximum z-coordinate at apoapsis. Sample transfers are indicated in the boundaries of the figure.

apogee along the departure and arrival tori, respectively. Each point in this two-dimensional space indicates that a feasible natural transfer is computed to satisfy the optimization problem summarized in Equation (7) with $f(\boldsymbol{X}) < 10^{-18}$ and $\|\boldsymbol{F}(\boldsymbol{X})\| < 10^{-12}$. Four sample transfers, labelled as A1

to A4, are also displayed. Each figure displays the Earth and the Moon as gray circles, together with the Earth-Moon Lagrange points as red diamonds. Each figure demonstrates that the overall transfer geometry is consistent throughout the family. However, as observed in the gray lateral xz- and yz-projections, each transfer connects quasi-periodic orbits with different out-of-plane displacements. For example, transfer A1 connects the last members of the 3:2 and 1:2 quasi-periodic orbit JC-families, which admit the largest out-of-plane displacement. For this reason, this transfer exhibits the largest out-of-plane motion. Conversely, transfer A3 connects the second members of these two families, representing an almost planar transfer. Transfer A2 starts from an almost planar 3:2 quasi-periodic orbit and approaches the last member of the arrival 1:2 quasi-periodic orbit family. Transfer A4 exhibits an initially relatively large out-of-plane displacement, culminating with almost planar motion. Analysis of Figure 8 reveals useful insights into the existence of natural transitions between quasi-periodic orbits within each family. Specifically, given a fixed initial quasi-periodic orbit near the 3:2 resonance, a transition only exists to selected quasi-periodic orbits near the 1:2 resonance and vice versa. The existence of these transitions, for this particular transfer geometry, appears to be linked to the relative difference in the maximum out-of-plane component along each quasi-periodic orbit. For initial quasi-periodic orbits near the 3:2 resonance with a small out-of-plane deviation, only tori near the 1:2 resonance with a small out-of-plane component are naturally accessible in the CR3BP. As the tori evolve along each family, natural transitions occur at a larger range of differences in the maximum out-of-plane components.

Computing the quasi-periodic orbits near each resonance using only an average Jacobi constant constraint, for a fixed discretization, enables an expanded exploration of the solution space associated with the natural transfer in Figure 6(a). Specifically, JC_A-families of quasi-periodic orbits are computed for each of the 1:2 and 3:2 resonances. Each of the computed tori is constrained to possess an average Jacobi constant $JC = 2.73$ across the invariant curve with $N = 25$ and $Q = 5$. Constraining the average Jacobi constant across the states sampled along the invariant curve, rather than constraining JC at all states, produces a wider range of members across the family for the same discretization. In fact, at the selected discretization, the last computed members of each JC_A-family possess a larger maximum out-of-plane extension at apogee than members of the JC-families, as shown in Figure 2. Using the computed ranges of tori, the point solution from Figure 6(a) is used to compute similar natural transitions between members of the JC_A-families of quasi-periodic orbits near each of the 1:2 and 3:2 resonances. These natural transfers satisfy the presented optimization problem with $f(\boldsymbol{X}) < 10^{-12}$ and $\|\boldsymbol{F}(\boldsymbol{X})\| < 10^{-12}$; during continuation, the Jacobi constant along the transfer is constrained to match only the average value along the tori. A summary of the existence of these natural transfers between quasi-periodic orbits in the JC_A-families near each of the 1:2 and 3:2 resonances is displayed in Figure 9 with a configuration that is consistent with Figure 8. This set of transfers that resemble the point solution in Figure 6(a) are calculated for a wider array of combinations of tori near each of the 3:2 and 1:2 resonances. Yet, the observation noted in the previous example still applies: the existence of these natural transitions, for this particular transfer geometry, appears to be linked to the relative difference in the maximum out-of-plane component along each quasi-periodic orbit. In addition, the presence of a close pass to the smaller primary likely contributes to the wide array of quasi-periodic orbits that admit a natural transition, even between tori with significant differences in the maximum out-of-plane component at apogee. Figure 9 displays four examples of the computed transfers at a combination of departure and arrival tori that are located by the red circles in the top-right plot. The left side of the figure reports transfers B1 and B2, associated with the last row of the top-right plot. These natural transitions connect the fifth and last member, respectively, of the departing 3:2 quasi-periodic orbit family to the last mem-

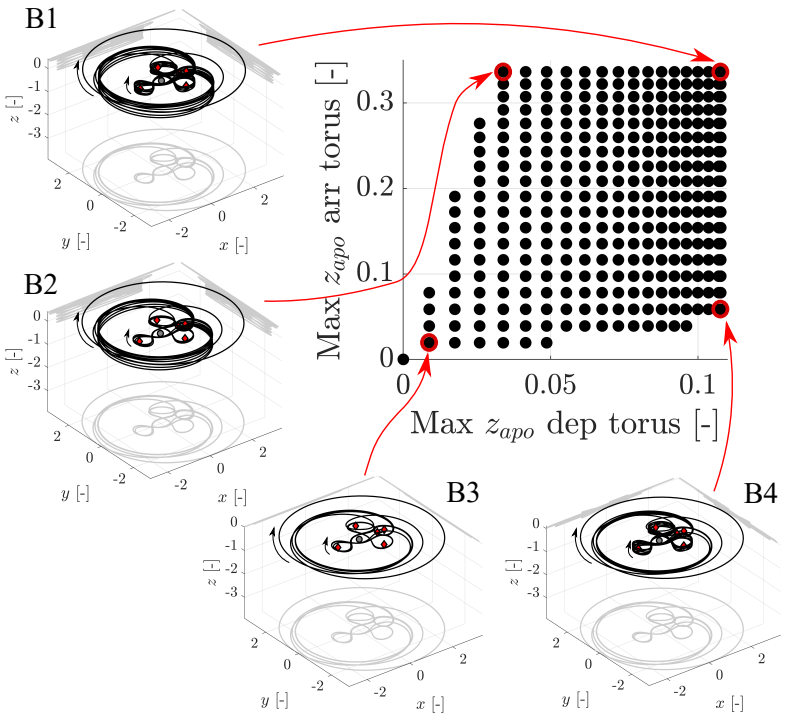

Figure 9. Summary of the T1 natural transfers continued from Figure 6(a). Each black marker indicates a transfer from a departing 3:2 quasi-periodic orbit and an arrival 1:2 quasi-periodic orbit in the JC_A-families, each identified by the maximum z-coordinate at apoapsis. Sample transfers are indicated in the boundaries.

ber of the arrival 1:2 quasi-periodic orbit family. Both transfers exhibit a large arrival out-of-plane motion: however, B1 admits a larger departing out-of-plane displacement when compared to B2. Transfers B3 and B4 are displayed on the bottom of Figure 9: B3 connects the second members of the quasi-periodic orbit families, exhibiting a small out-of-plane motion. Transfer B4 connects a large out-of-plane departing torus to an almost planar arrival 1:2 quasi-periodic orbit, as highlighted by the xz- and yz-projections. Since a low-amplitude arrival quasi-periodic orbit is targeted, the arc connecting the departing and arrival quasi-periodic orbit for transfers B3 and B4, which extends far from the Earth, tends to lie close to the xy-plane, unlike transfers B1 and B2 where the connecting arc admits a large out-of-plane displacement. Nevertheless, each transfer exhibits a similar geometry of the planar projection, consistent with the point design displayed in Figure 6(a).

Analysis of the existence of natural transfers with a similar geometry to the T2 transfer in Figure 6(b) is performed for the JC-families of quasi-periodic orbits at $JC = 2.73$ near the 3:2 and 1:2 resonances. This point solution naturally connects the last computed members of the JC-family near the 3:2 and 1:2 resonances. However, this transfer exhibits a distinct geometry from the previous example: the test particle spends more time in proximity of the L_4 and L_5 points before approaching the 1:2 quasi-periodic orbit. Continuation is used to compute similar natural transfers between members of each family, with the results summarized in Figure 10 using a configuration consistent with Figure 8. Each colored point represents a viable natural transfer with $f(\boldsymbol{X}) < 10^{-18}$ and $\|\boldsymbol{F}(\boldsymbol{X})\| < 10^{-12}$, with a similar geometry to Figure 6(b). Two natural transfers are highlighted in the figure: the bottom-right transfer naturally connects two tori with a relative low out-of-plane component, while the top transfer connects two tori with a significant out-of-plane extension. Anal-

ysis of Figure 10 reveals that these transfers exist across a smaller range of the two families than in the previous example. Such an observation is likely due to the absence of a close pass to the smaller primary in this particular type of transfer. In fact, the existence of natural transitions between spatial quasi-periodic orbits near two distinct resonances appears to be influenced by the transfer geometry.

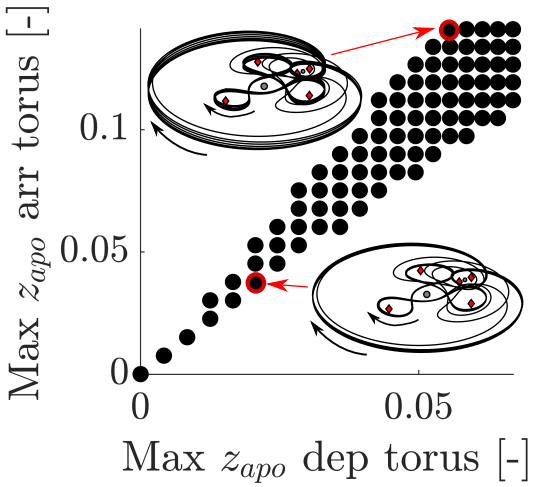

Figure 10. Summary of the T2 natural transfers continued from Figure 6(a). Each black marker indicates a transfer from a departing 3:2 quasi-periodic orbit and an arrival 1:2 quasi-periodic orbit in the JC-families, each identified by the maximum z-coordinate at apoapsis. Sample transfers are indicated in the boundaries of the figure.

CONCLUDING REMARKS

Natural transitions between quasi-periodic orbits that exist near resonances in the Earth-Moon CR3BP are computed and analyzed. First, families of quasi-periodic orbits are computed at a fixed value of the Jacobi constant near two resonances: the 3:2 and 1:2 resonances. Then, the associated hyperbolic invariant manifolds are generated for two members of each family: the unstable manifold associated with a quasi-periodic orbit near the 3:2 resonance and the stable manifold associated with a quasi-periodic orbit near the 1:2 resonance. Each trajectory along a manifold is reduced to a discrete sequence of points and examined via a Poincaré map. This multi-dimensional dataset, comprised of the intersections of these manifolds with a surface of section, is challenging to visualize on a traditional two- or three-dimensional projection composed of the phase space variables. Thus, Uniform Manifold Approximation and Projection, a form of manifold learning used for dimension reduction, is leveraged. Specifically, each four-dimensional manifold crossing is projected onto a two-dimensional Euclidean manifold. This projection enables straightforward visualization of the data and a rapid analysis to construct an initial guess for a natural transfer formed using trajectories on the unstable and stable manifolds. In the projected space, nearby crossings from each manifold structure in distinct regions are used to construct initial guesses for transfers with distinct properties. A numerical correction procedure is then used to recover nearby continuous solutions. Two of these point solutions are used in a continuation scheme to calculate natural transitions with a similar geometry between other members of the computed families of quasi-periodic orbits. Studying the existence and properties of these natural transitions between quasi-periodic orbits that exist near resonances enables an expanded analysis of the general phenomenon of resonance transition

in multi-body gravitational environments; such insight is valuable in both trajectory design and celestial mechanics. In fact, analysis of the expanded solution space associated with resonance transitions in the CR3BP may supply insight into the dynamical mechanisms governing the long-term behaviour of spacecraft trajectories, comets and Kuiper belt objects in higher fidelity models.

REFERENCES

[1] Carrico, J Jr.; Dichmann,D.; Policastri, L.; Carrico, J. III; Craychee, T.; Ferreira, J.; Intelisano, M.; Lebois, R.; Loucks, M.; Schrift, T.; Sherman, R., "Lunar-Resonant Trajectory Design for the Interstellar Boundary Explorer (IBEX) Extended Mission," *Advances in the Astronautical Sciences*, Vol. 142, December 2011, pp. 771 – 789.

[2] Dichmann, D; Parker, J; Nickel, C.; Lutz, S., "Trajectory Design for the Transiting Exoplanet Survey Satellite," *International Symposium on Spacecraft Flight Dynamics*, Laurel, MD, May 2014.

[3] Short, C; Howell, K.C.; Haapala, A.; Dichmann, D., "Mode Analysis for Long-Term Behavior in a Resonant Earth-Moon Trajectory," *Journal of the Astronautical Sciences*, Vol. 64, 2017, pp. 156 – 187.

[4] Koon, W. S.; Lo, M. W.; Marsden, J. E.; Ross, S. D, "Resonance and Capture of Jupiter Comets," *Celestial Mechanics and Dynamical Astronomy*, Vol. 81, No. 27, September 2001, pp. 27 – 38, 10.1023/A:1013398801813.

[5] Lykawka, P.S.; Mukaia, T., "Resonance sticking in the scattered disk," *Icarus*, Vol. 192, 2017, pp. 238 – 247.

[6] Haapala, A.F.; Howell, K.C., "Trajectory Design Strategies Applied to Temporary Comet Capture Including Poincaré Maps and Invariant Manifolds," *Celestial Mechanics and Dynamical Astronomy*, Vol. 116, 2013, pp. 299 – 323.

[7] Z. Olikara, *Computation of Quasi-Periodic Tori and Heteroclinic Connections in Astrodynamics Using Collocation Techniques*. PhD thesis, University of Colorado Boulder, Boulder, Colorado, 2016.

[8] Á. Jorba, "Numerical Computation of the Normal Behavior of Invariant Curves of n-Dimensional Maps," *Nonlinearity*, Vol. 14, No. 5, 2001, pp. 943 – 976.

[9] McInnes, L.; Healy, J.; Melville, K., "UMAP: Uniform Manifold Approximation and Projection for Dimension Reduction," arXiv:1802.03426, (9 February 2018).

[10] Cao J.; Spielmann, M.; Qiu, X.; Huang, X.; Ibrahim, D.M.; Hill, A.J.; Zhang, F.; Mundlos, S.; Christiansen, L.; Steemers, F.J.; Trapnell, C.; Shendure, J., "The Single-Cell Transcriptional Landscape of Mammalian Organogenesis," *Nature*, Vol. 566, 2019, pp. 496 – 502.

[11] Diaz-Papkovicha, A.; Anderson-Trocmé, L.; Ben-Eghan, C.; Gravel, S., "UMAP Reveals Cryptic Population Structure and Phenotype Heterogeneity in Large Genomic Cohorts," *PLos Genetics*, Vol. 15, No. 11, 2019, 10.1371/journal.pgen.1008432.

[12] Bloch, T.; Watt, C.; Owens, M.; McInnes, L; Macneil, A.R., "Data-Driven Classification of Coronal Hole and Streamer Belt Solar Wind," *Solar Physics*, Vol. 295, No. 41, 2020.

[13] V. Szebehely, *Theory of Orbits: The Restricted Problem of Three Bodies*. London, UK: Academic Press, 1967.

[14] Murray, C.D.; Dermott, S.F, *Solar System Dynamics*. Cambridge: Cambridge University Press, 1999.

[15] Anderson, R.L.; Lo, M.W., "Dynamical Systems Analysis of Planetary Flybys and Approach: Planar Europa Orbiter," *Journal of Guidance, Control, and Dynamics*, Vol. 33, No. 6, 2010, 10.2514/1.45060.

[16] Barrabés, E.; Gómez, G.., "Spatial p-q Resonant Orbits of the RTBP," *Celestial Mechanics and Dynamical Astronomy*, Vol. 84, 2002, p. 387 – 407.

[17] L. Perko, *Differential Equations and Dynamical Systems, 3rd Edition*. New York: Springer, 2000.

[18] F. Verhulst, *Nonlinear Differential Equations and Dynamical Systems*. Berlin, Heidelberg: Springer-Verlag, 1996, 10.1007/978-3-642-61453-8.

[19] Baresi, N., Olikara, Z.P., Scheeres, D.J., "Fully Numerical Methods for Continuing Families of Quasi-Periodic Invariant Tori in Astrodynamics," *Journal of Astronautical Sciences*, Vol. 65, No. 27, 2018, pp. 157 – 182.

[20] Gómez, G., Mondelo, J.M., "The Dynamics Around the Collinear Equilibrium Points of the RTBP," *Physica D*, Vol. 157, No. 4, 2001, pp. 283 – 321.

[21] Gómez, G.; Koon, W.S.; Lo, M.W.; Marsden, J., "Connecting orbits and invariant manifolds in the spatial restricted three-body problem," *Nonlinearity*, Vol. 17, 2004, pp. 1571 – 1606.